Received: 11 October 2024 | Revised: 11 July 2025 | Accepted: 5 August 2025 | Published online: 26 September 2025

RESEARCH ARTICLE

Journal of Computational and Cognitive Engineering
2026, Vol. 5(1) 30–43
DOI: 10.47852/bonviewJCCE52024527

BON VIEW PUBLISHING

A 3D Irrigation Canal Alignment Optimization Model for a Steep-Sloping Area with Rectangular Inclined Drops

Mehdi Kazemi[1], Ebrahim Amiri Tokaldani[1], Manoj K. Jha[2,*], and Ramesh Rudra[3]

[1] *Department of Irrigation and Reclamation Engineering, University of Tehran, Iran*

[2] *Department of Information Technology, University of Maryland Global Campus, USA*

[3] *School of Engineering, University of Guelph, Canada*

Abstract: Traditional optimization approaches for irrigation canal design have primarily focused on identifying cost-effective structural dimensions for simple cross-sections. However, these methods are inadequate for steep terrains where the construction of single or multiple rectangular inclined drops (RIDs) becomes essential. This study introduces a novel three-dimensional optimization model tailored for the optimal design of irrigation canals in such challenging environments. By integrating geospatial data with a particle swarm optimization (PSO) algorithm, the model establishes a continuous search space that facilitates the identification of cost-effective alignments while satisfying hydraulic and construction constraints. To validate its effectiveness, the model was applied to two synthetic case studies that feature varied terrain and slope conditions. Results demonstrated the model's strong capability in optimizing both canal alignment and RID placement. Comparative analysis with genetic algorithm and ant colony optimization revealed that PSO outperformed both in terms of solution accuracy and consistency. Moreover, the proposed model produced results comparable to conventional design methods but with significantly reduced computational time. In addition, pre-cost-estimation tables were developed for various canal route alternatives and RID configurations, offering practical insights for efficient planning and preliminary design of irrigation canals in complex, sloping regions.

Keywords: three-dimensional canal route alignment, rectangular inclined drop, optimization, PSO algorithm, canal optimization

1. Introduction

The design and implementation of a canal route in steep lands with a single drop or a set of drops are challenging problems. Similar to optimizing highway or rail alignments, they involve time-consuming design-related tasks due to various operational, hydraulic, and economic constraints [1]. In general, the use of intertwining parameters in the conventional design of the canal routes, which include various hydraulic structures, requires experienced engineers. It is time-consuming to find an optimal canal route due to an infinite number of possible routes [2] and positions to locate the hydraulic structures between specified starting and ending points. Hence, it is strongly desired to consider all alternatives for canal routes and the number and location of the hydraulic structures—preliminarily designed and compared with each other—to find the best solution from economic and technical points of view. Surprisingly, in traditional design, it is only possible to consider a very limited number of route options [3–5] and perform design calculations—only for the selected alternative. Therefore, it is essential to develop an intelligent model in the substrate of factual information by taking into account the costs in the design and construction of the canal route [6] and its related hydraulic structures.

Developing an automated model to determine the optimal canal route, flow section dimensions, and the number and height of rectangular inclined drops (RIDs) while accounting for hydraulic and economic constraints between two specified points using geospatial data has long been a priority for researchers and engineers. Addressing these factors is essential for producing reliable, real-world solutions. Since the 1980s, much research has been carried out to determine the optimal dimensions of the flow section along a canal route [7–11]. The implicit and combined structure of the cost function or constraints, as well as solving nonlinear optimization problems in determining the optimal dimensions of the flow section, has led to the widespread use of heuristic and metaheuristic methods [12]. Swamee et al. [13] developed an explicit design equation and the shape factor of rectangular, trapezoidal, and circular sections using a nonlinear optimization method. They calculated the optimal dimensions of the canal to minimize the execution cost and reported that the use of their method was appropriate in the early stages of design. Jain et al. [14] solved the aforementioned explicit design equation using a genetic algorithm (GA) and found that consideration of the velocity constraint led to a 55% reduction in cost. However, the cost saving was only 35% without considering the velocity constraint. Depeweg and Urquieta [15] designed an irrigation canal by combining GIS and Elvis software. They obtained a 300 m reduction in the length of the canal and 10% of the total earthwork volume compared to the traditional design method. Aksoy and Altan-Sakarya [16] as well as Turan and Yurdusev [17] obtained the acceptable values of the width, depth, and side slope of the canal using the analytical solution method and the evolutionary difference algorithm, respectively. Furthermore, they reported that their algorithms were reliable. Tofiq and Guven [18]

*Corresponding author: Manoj K. Jha, Department of Information Technology, University of Maryland Global Campus, USA. Email: manoj.jha@faculty.umgc.edu

calculated the width-to-depth ratio for minimizing the construction cost of a water transmission canal using genetic programming and reported that the use of the proposed method led to a reduction of approximately 30% of the cost compared to using conventional methods. El-Ghandour et al. [19] used the particle swarm optimization (PSO) algorithm to determine the optimal dimensions of the canal to minimize earthwork costs by considering leakage and evaporation constraints. They reported that the use of the proposed method led to 28% to 41% reduction in total cost compared to the traditional approach.

Previous studies have focused on the geometric optimization of canal cross-sections, such as trapezoidal, rectangular, and parabolic shapes, to achieve efficient water conveyance while minimizing the wetted perimeter and seepage losses. Although numerical, analytical, and empirical methods have been developed to determine optimal canal dimensions, they are often limited to a one-m section and fail to account for critical factors such as soil type and land topography—both of which are essential in the design of effective irrigation canals [20]. Analyzing complex terrain—particularly areas with significant elevation changes—is challenging to perform manually and often results in inefficient or impractical canal alignments. Traditional methods are resource-intensive, requiring extensive field studies that demand substantial time, effort, and financial investment, especially over large areas. Furthermore, these conventional approaches typically evaluate only a limited set of route alternatives, which increases the risk of selecting a suboptimal alignment. As a result, the solutions derived from such methods cannot be reliably considered optimal or even feasible for real-world implementation. In practical applications, an optimized canal route must be location-specific, accounting for both alignment and volume-related construction factors. Therefore, any applicable optimization model must incorporate both horizontal and vertical optimizations. Horizontal optimization, in particular, requires a wide range of detailed information, including soil type, land use, topographic maps, and other geospatial data [21–26]. The main task of horizontal optimization models is to determine the optimal canal crossing route based on the geospatial information used in the model. The vertical optimization model is developed with the aim of evaluating the cost of earthworks, transportation, and controlling the longitudinal slope of the route [27–29]. To arrive at a realistic and truly optimal solution, it is essential to simultaneously optimize both the horizontal and vertical alignments—an approach known as a three-dimensional (3D) optimization model [30]. 3D optimization models use different metaheuristic algorithms integrated with a geospatial or geographic information system (GIS) as a search space [31, 32]. In this integrated approach, the algorithm generates random alignment paths, simultaneously evaluates the associated horizontal and vertical costs, and selects the option with the lowest total cost that complies with engineering constraints. Although numerous studies have explored 3D optimization—particularly in the context of highway and railway design—those investigations lie beyond the scope of this study. Nevertheless, they consistently validate the method's practicality and effectiveness in real-world alignment planning [1, 22, 33–36].

The literature review highlights that determining the optimal canal alignment and the strategic placement of RIDs necessitates the development of an automated model capable of evaluating alternatives from economic, technical, and hydraulic perspectives. Accordingly, this research presents an intelligent optimization model integrated with geospatial data to design efficient canal routes in steep-slope terrains, where the incorporation of RIDs is essential.

2. Canal Alignment Optimization Model

The proposed canal alignment optimization model has four components: layers of geographical information, an objective function, hydraulic and executive constraints, and design variables. These components will be discussed in detail in the subsequent sections.

3. Canal Costs

As the proposed model aims to identify the most economically optimal canal route incorporating RID sets, it is essential to accurately define the cost components associated with canal construction. The total construction cost can be broadly categorized into four types: (1) length-dependent costs, (2) volume-dependent costs, (3) location-dependent costs, and (4) construction-dependent costs. Each type of cost may influence the optimal alignment differently—for instance, construction-dependent costs favor minimizing the number of RIDs, whereas volume-dependent costs may favor increasing them along certain alignments. Therefore, a comprehensive and precise cost formulation is necessary to effectively optimize the canal route by minimizing the total cost.

3.1. Length-dependent cost

The length-dependent cost includes lining and trimming, which is calculated by multiplying the cost of the unit length of the canal along the route.

$$C_{Len} = K_{Len} \times L, \tag{1}$$

where K_{Len} is the total cost of the lining and trimming for 1 m of canal length and L is the total length of the route.

3.2. Volume-dependent cost

Volume-dependent costs are construction expenses that change in proportion to the amount of material excavated, moved, or placed in canal projects. These costs are primarily associated with earthwork activities and hauling. As they directly relate to the physical volume of work, accurate estimation is essential for effective planning and cost control in infrastructure development.

3.3. Earthwork cost

The volumes of embankment and excavation are calculated using the average end area between two consecutive station points. At these points, the bed elevation of the canal is calculated using Equation (2). The terrain level is also extracted from the corresponding matrix of the rasterized elevation map.

$$Z_{C_j} = Z_{PI_i} + L_{S_j} \frac{Z_{PI_i} - Z_{PI_{i+1}}}{L_{V_i}}, \tag{2}$$

where Z_{C_j} is the elevation of the canal bed at the jth station point, Z_{PI_i} and $Z_{PI_{i+1}}$ are the elevations of two consecutive intersection points, L_{S_i} is the distance from the jth station point to the intersection point, and L_{v_i} is the horizontal distance of the PI points from the beginning of the route. On the basis of the elevation of the canal bed, the terrain elevation at the station points, and the determination of excavation or fill in that section, the area of consecutive sections is calculated and the volume of each type of earthwork (cut or fill) is obtained. Figures 1–3 show the cross-section of the canal in the state of excavation, embankment, and simultaneous excavation and embankment, respectively.

The equations below are used to determine the volume of earthwork and its total cost.

$$E_N = (E_{cw} + E_c) - \lambda E_f, \tag{3}$$

Figure 1
The view of cutting cross-section

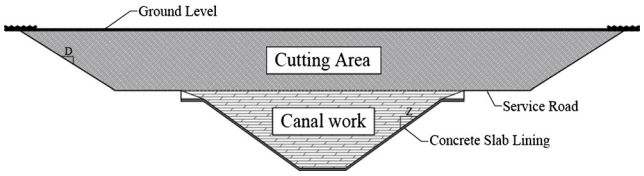

Figure 2
The view of filling cross-section

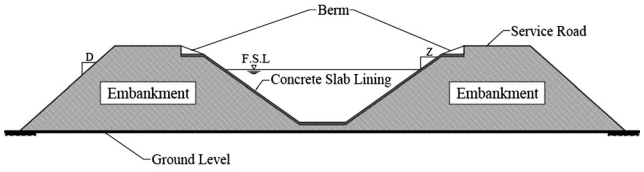

Figure 3
The view of transition cross-section (cut & fill)

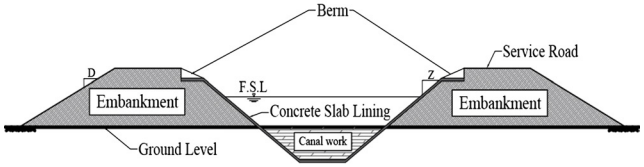

$$C_{vol} = K_c \times E_c + K_{cw} \times E_{cw} + K_f \times E_f + K_l \times max(E_N, 0) - K_b \times min(E_N, 0) \quad (4)$$

where E_N, E_c, E_f, and E_{cw} are the net volumes of earthwork, cutting, embankment, and soil related to canal works, respectively; K_c, K_f, and K_l are the costs per cubic meter of excavation, embankment, and canal works, respectively; K_l is the transportation cost for moving 1 m^3 of soil to the landfill; K_b represents the cost of transporting 1 m^3 of soil from the borrow pit; C_{vol} is the total cost related to the volume; and λ is the expansion coefficient of the soil.

3.4. Construction-dependent cost

The costs related to the construction include the costs for constructing each hydraulic structure along the canal route, limited only to the costs for RIDs. After the determination of each RID's and stilling pool's dimension, construction cost, including reinforcement (C^{reinf}), concreting (C^{cncrt}), and framework (C^{fw}), is calculated for each of the structures separately using Equation (5).

$$C_{Cons} = \sum_{i=1}^{n} \left(C_{Drop}^{reinf} + C_{Drop}^{cncrt} + C_{Drop}^{fw} \right) \times L_{Drop}(i) + \left(C_{Basin}^{reinf} + C_{Basin}^{cncrt} + C_{Basin}^{fw} \right) \times L_{Basin}(i) \quad (5)$$

where $L_{Drop}(i)$ and L_{Basin} are the length of the ith drop and its stilling pool, respectively.

3.5. Location-dependent cost

One of the most critical factors in determining the cost of a canal route is the location-dependent cost, which reflects variations in soil type, land use, and restrictions on canal passage through certain areas. This cost quantifies the cumulative expense associated with traversing each location, enabling the optimization algorithm to identify the most cost-effective route. By incorporating location-dependent costs, planners can design economically viable alignments that also comply with technical and environmental constraints.

4. Model Development

4.1. Data processing and information layers

Optimizing canal alignment requires the integration of GIS tools and spatial data to effectively balance technical and economic considerations. The process begins by clearly defining the alignment objectives—such as minimizing construction costs—while satisfying constraints such as avoiding environmentally protected zones or areas with unsuitable soil conditions. To support this goal, relevant GIS layers are collected, including topography, soil type, land use, and other critical factors influencing route selection. All datasets are standardized to a common coordinate system to ensure spatial consistency. When maps are available only in hard copy, they are digitized and rasterized, and each layer is assigned a weight to represent its relative importance in the decision-making process. In Figure 4, zones with different land uses and characteristics are digitized (Figure 4(a)) and valued (Figure 4(b)) based on the available information layers. The valuation of each zone is determined either by its actual economic cost or by the user's judgment regarding its suitability for canal passage. To enhance computational efficiency, the spatial data are rasterized and stored in a matrix format, representing the entire search space. Each matrix cell traversed by the proposed canal route contains digitized attributes, including elevation data, descriptive information, and the assigned cost valuation.

Figure 4
(a) Digitizing and (b) valuating the search space

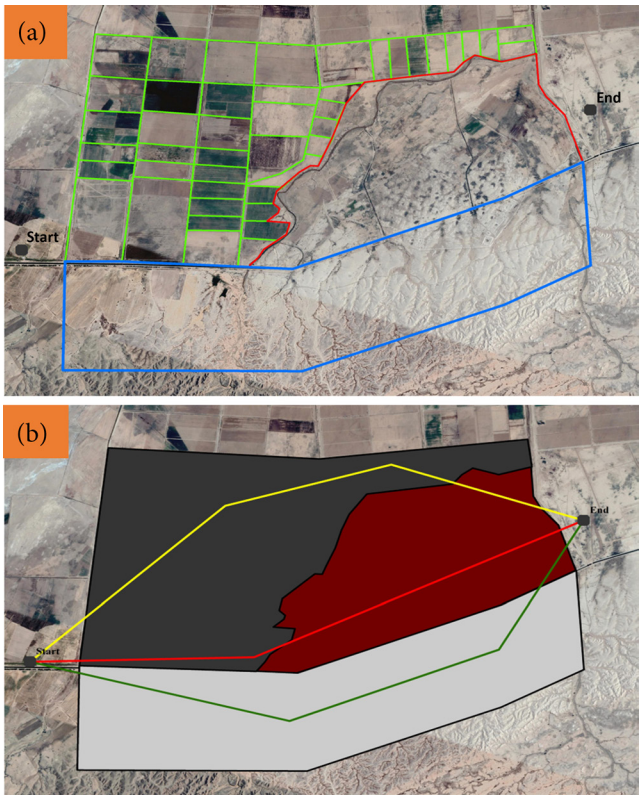

4.2. Definition of 3D alignment

This research aims to develop a 3D intelligent optimization model for canal route alignment in steep-sloping terrains, where the inclusion of RIDs is essential. By incorporating multiple geospatial data layers into a continuous search space, the resulting alignments are expected to be more practical and representative of real-world conditions—offering a significant improvement over previous studies that focused solely on optimizing cross-sectional parameters. The alignment is defined by a series of intersection points in 3D space, referred to as cutting plans. These points are generated randomly, and a continuous 3D trajectory is established by connecting the start and end points of the canal route through these intermediate points. To speed up the optimization process, after the determination of 2D alignment (Figure 5(b)), the height parameter of the intersection points (Zi) is updated by applying a random longitudinal slope to the existing route. At this stage, A 3D-inclined path with a standard longitudinal slope (0.0005–0.001 for lined canals) is constructed with an epsilon distance to the endpoint (see the initial path in Figure 5(a)). Now the route consists of a specific number of tangents (loci), each of which has a unique number (Figure 5(b)). To optimally place each RID along a canal route, it is necessary to consider the maximum allowable number of RIDs. By choosing the highest number of drops at the beginning of the optimization, lower numbers can be achieved at the end of the process. The initial number of drops can be determined in three different ways: 1) user experience, 2) hydraulic consideration of the distance between successive drops, and 3) choosing the highest number of drops with the lowest standard height. Here, the number of each tangent (loci) is randomly generated, and the standard slope of the inclined part (2H:1V or 1.5H:1V) is applied to each tangent. Accordingly, at each iteration of the optimization algorithm, a set of RIDs with different slopes and heights is placed in different locations on the route (see Figure 5(a), drops in i'th and j'th iterations). Figure 6 shows the process, input, and output values of the 3D optimization model for determining the route of the canal and the set of RIDs. The spatial information of each alignment is encoded into a matrix format, and the dominant cost components are assessed in the PSO module. Each alignment candidate is evaluated using an objective function, and the movement of each particle is guided by both its own best-known position (local best) and the overall best position found by the swarm (global best) based on the minimum construction cost. This evolutionary process is repeated iteratively until the best global solution shows no significant improvement over a predefined number of iterations.

4.3. Coordinate system

Spatial information is extracted from georeferenced maps stored in standardized coordinate systems. For computational simplicity, this research employs a local coordinate system. Given the critical role of terrain elevation in estimating construction costs—particularly for earthworks—and in defining the canal alignment, coordinate transformation is applied only in two dimensions. The local system is defined such that the origin is set at point (0, 0, Z), and the coordinate values extend along the X and Y axes [4].

Figure 5
Basic parameters of the proposed model for path generation and placing the RIDs throughout the vertical alignment

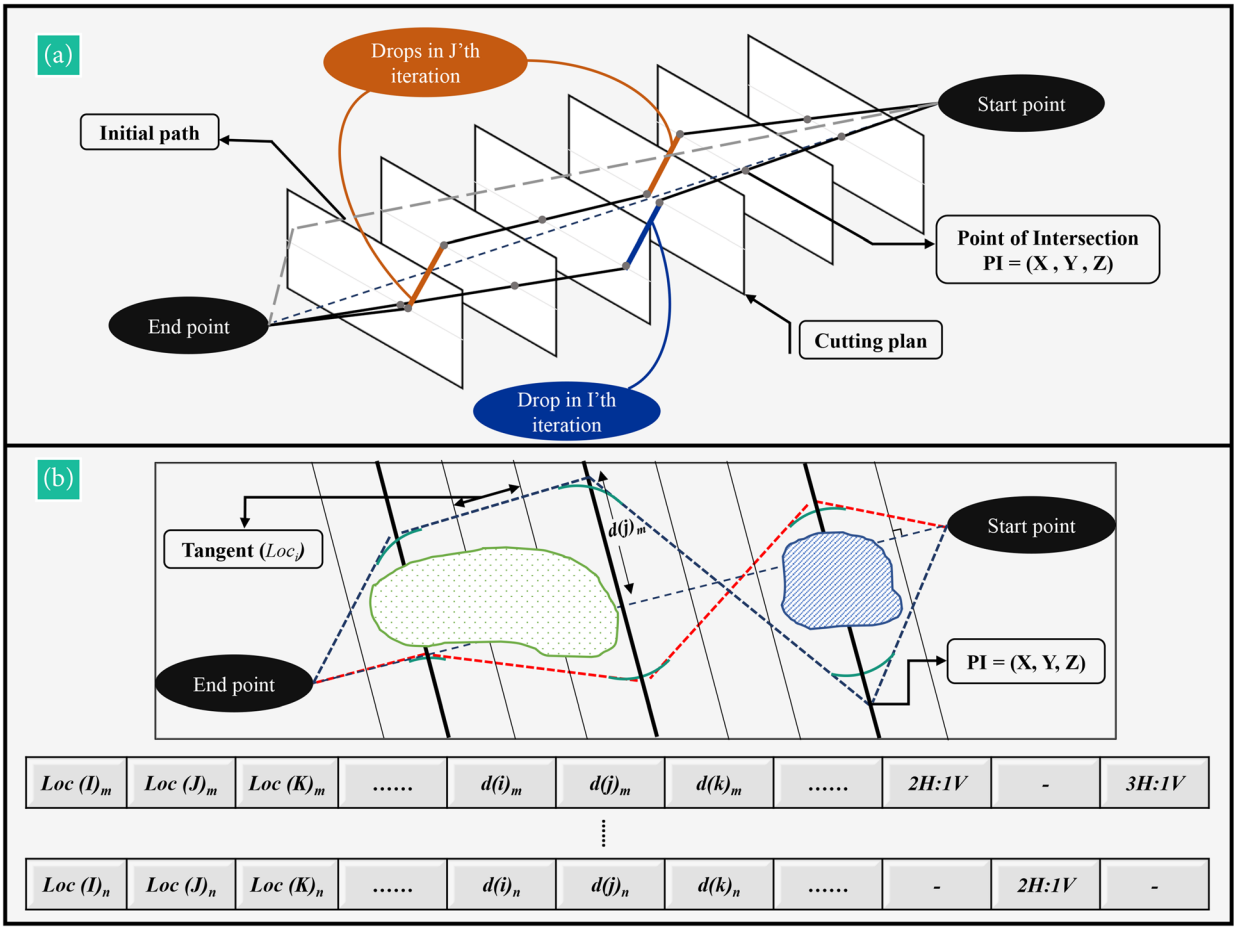

Figure 6
Structure of the proposed model for canal and drop set alignment optimization using the PSO algorithm

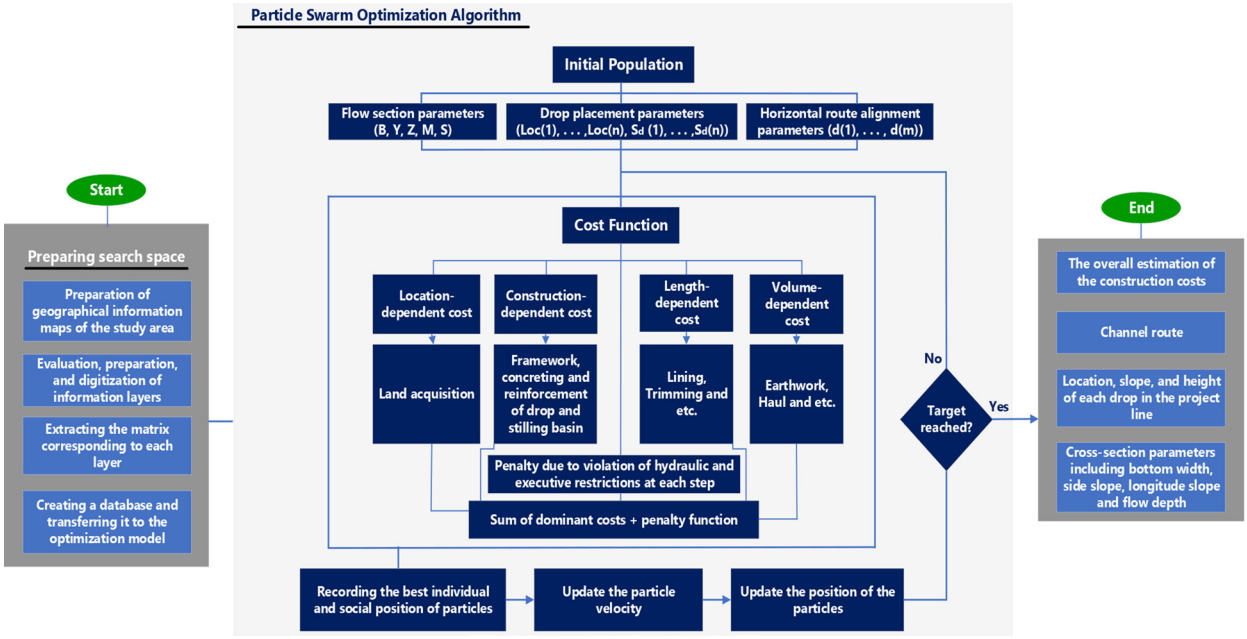

4.4. Constraint handling

The 3D optimization model for determining the canal alignment and the placement of RIDs is designed to minimize the total construction cost while adhering to established design standards. These standards are incorporated into the model as constraints. This section outlines the hydraulic and operational (executive) constraints that influence the selection of the canal route, the dimensions of the flow cross-section, and the positioning and elevation differences of the RIDs.

4.4.1. Manning equation and Froude number

The Manning formula, also known as Strickler's equation, has been proven to be the most reliable in designing fluid flow sections [37]. This equation has been used in this research to design the flow section across the canal route. The values of the longitudinal slope, side slope, depth, and width of the flow section are generated by the algorithm and inserted into Equation (6). Equation (6) is expressed as follows:

$$Q = \frac{1}{n}.A.R^{\frac{2}{3}}.S^{\frac{1}{2}}, \tag{6}$$

where A and R represent the flow area and hydraulic radius, respectively, which are functions of the canal's bed width, flow depth, and side slope. S and n are the longitudinal slope and Manning's roughness coefficient, respectively. To achieve the expected flow rate, the difference between the flow rate obtained by the model and the design discharge is found by magnifying this difference using two user-defined coefficients, namely, α and β. It is expressed as follows:

$$Cp_{manning} = \alpha\left[\left|Q_{design} - \frac{1}{n}.A.R^{\frac{2}{3}}.S^{\frac{1}{2}}\right|\right]^{\beta}. \tag{7}$$

The Froude number describes different flow regimes of the open channel flow, which is considered a limitation in determining the flow velocity. It is expressed as follows:

$$Fr = \frac{v}{\sqrt{gD}}, \tag{8}$$

where D, V, and g are the hydraulic radii, flow velocity, and gravity force, respectively.

4.4.2. Drops and basin elevation

The RID is a widely used regulatory structure to reduce the water level and to dissipate excess water energy using its stilling basin located after the inclined section. This structure has a rectangular section to transfer water from a higher to a lower elevation [38]. It is designed and implemented with a height difference of 1–5 m in unlined canals and 1–8 m in concrete canals. Using Equations (9) and (10), the bottom width of the inclined part (in meters) for RIDs and stilling basin is obtained for discharge up to and greater than 3 m3/s, respectively. Notably, to obtain Equation (10), it is assumed that the upstream depth (H_{max}) does not exceed 1.5 m in height.

$$b_d = \frac{18.46\sqrt{Q}}{9.91+Q}, \tag{9}$$

$$b_d = \frac{Q}{1.7H_{max}^{1.5}}, \tag{10}$$

where b_d is the width of the inclined drop and its stilling basin (m), and Q is the discharge (m^3/sec). The location and distance between two consecutive drops are determined according to economic and hydraulic considerations. From an economic perspective, the distance between drops should balance embankment and excavation, considering the density of the local soil and the canal body [39]. Economic advantage also plays a vital role in choosing the number and height of drops. More drops with lower heights reduce the volume of earthworks and increase the construction costs of structures and vice versa [39]. From a hydraulic perspective, water surface elevation is required for water intake. An adequate space for the development of uniform flow should be provided [38]. Empirically, the minimum distance between two consecutive drops for a flow of up to 3 cms is 60 m. Therefore, a height difference of up to 8 m in the lined channels and a distance of 60 m between consecutive drops for the flow of up to 3 m^3/sec are applied as control restrictions [40]. The basis for determining the distance between two successive drops for higher flow rates is the distance required to

fully form the M2 water surface profile. If the profile does not extend, a control notch or other types of regulatory structures would be used to adjust the water level. A penalty function Cp_{elv} is applied to the 3D model to prevent the reverse slope at the end of the path. Following this approach, the net difference between the height of the starting point and the end of the path minus the sum of the heights of the drops and the height difference caused by the longitudinal slope of the canal is penalized in a magnified way. Equation (11), as presented below, ensures that the longitudinal slope and height difference of the routes are within feasible bounds.

$$Cp_{elv} = \alpha\left[\,\Delta(Elv_{start} - Elv_{End}) - S \times L - \sum_{i=1}^{n} Z_{Drop}(i)\right]^{\beta}, \quad (11)$$

where α and β are user-defined coefficients, S is the longitudinal slope, L is the total canal route length, Elv_{start} and Elv_{End} are the elevation of the starting and ending points of the path, respectively, and $Z_{Drop}(i)$ is the height difference of each of the RIDs.

5. Research Methodology

5.1. PSO algorithm

The PSO algorithm is a widely used evolutionary algorithm for solving optimization problems involving continuous and nonlinear functions [3, 41–44]. The goal of an optimization process is to find the best solution of a given optimization problem without violating the prescribed constraints [45]. In a PSO algorithm, an optimization technique is proposed with the option of changing the velocity of the particles in each iterative step to achieve the best individual and social position [46]. The basis of this algorithm is that each particle adjusts its location according to the best location that it has ever been and the best location in its entire neighborhood. In the present research, the PSO algorithm has been employed using a constriction factor introduced by Clerc [47]. The velocity vector and position of each particle are updated using Equation (12) and Equation (13) to minimize the fitting function. These equations are expressed as follows:

$$\begin{aligned} V_i(t+1) = w[V_i(t) + C_1 r_1[X_{lb,i}(t) - X_i(t)] \\ + C_2 r_2[X_{gb}(t) - X_i(t)]] \end{aligned} \quad (12)$$

$$X_i(t+1) = X_i(t) + V_i(t+1), \quad (13)$$

where W is the inertia weight, C_1 and C_2 are acceleration constants, r_1 and r_2 are randomly distributed matrices, $X_{lb}(t)$ and $X_{gb}(t)$ are the best local and global positions of the particles at time t, and $V_i(t+1)$ and $X_i(t+1)$ are the velocity and location of particle i at time $(t+1)$, respectively. Finding a balance between exploration and exploitation is essential for the algorithm to be able to find the best position [48]. The inertia weight, W, has always been considered an essential parameter in PSO, which significantly improves the exploration–exploitation trade-off [49]. Choosing a significant value of inertia weight increases the exploration, whereas a lower value leads to an increase in the exploitation ability. The scale and unit variation of the variables in the PSO algorithm require a delicate balance of the sensitivities of the variables. The flexibility in adjusting the parameters [50], convergence speed and simplicity [51], and ensuring the continuity of the search space have led us to use the PSO algorithm as an efficient tool to achieve the goals in the present research.

6. Summarized Optimization Model

The optimal design of the canal route requires the use of one or more RIDs in finding the least expensive feasible variant while considering the design, technical, and operational limitations. This requires successive evaluation and refinement of costs related to construction, volume, location, and length. Ultimately, the optimal placement and dimensions of the RIDs, the flow section dimensions, and the canal route are determined.

The final 3D alignment optimization model is formulated as follows:

$$Minimize\ C_{total} = C_{Loc} + C_{Vol} + C_{Len} + C_{Cons} + C_P$$

Subject to:

$$\begin{aligned} & d_L(i) \le d(i) \le d_U(i) \\ & 0.0005 \le S \le 0.001 \\ & 0.4 \le Fr \le 0.6 \\ & 1 \le Z_{Drop}(i) \le 8. \end{aligned} \quad (14)$$

The objective function includes the location-dependent cost (C_{Loc}), length-dependent cost (C_{Len}), volume-dependent cost (C_{Vol}), construction-related cost (C_{Cons}), and penalty function (C_P). In addition, $d_L(i)$ and $d_U(i)$ are the lower and upper limits of the search space, and Z_{Drop} is the allowable range of the drop height in the lined channel.

7. Numerical Examples

To verify the model's ability to calculate the optimal design of canal routes and the number of RIDs, two artificial examples and a real-world example are discussed. A stopping criterion of 300 iterations is defined for convergence based on an empirical observation that no significant improvement in the objective function is noted beyond 300 iterations.

7.1. Example 1

In example 1, a route was created with a height difference of 18.6 m at a distance of 400 m. Along the route, three height jumps of 5, 2, and 3 m are made at nearly identical intervals. Considering such variations in the terrain would help us understand whether the placement of drops is optimal. Figure 7 shows the perspective view of the artificial terrain.

After applying the initial parameters in the proposed model, including the costs and the design standards (see Table 1), the model starts the optimization process with the maximum allowable number of drops and the lowest height difference. Figure 8 shows the improvements over successive iterations in the early (a) and intermediate (b) steps

Figure 7
Perspective view of the elevation map of example 1

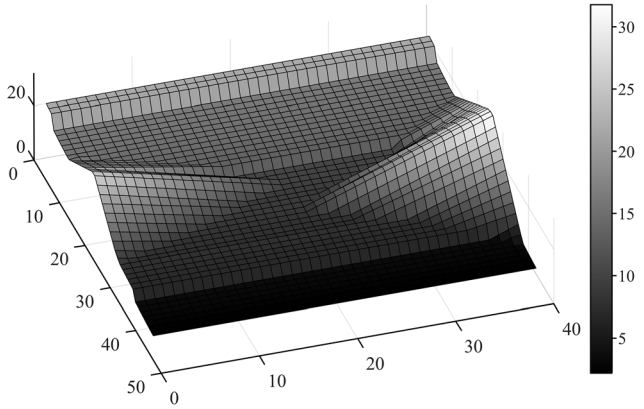

Table 1
Research gaps

Value	Item		
3 (m^3/s)	Discharge		
0.014	Manning coefficient		
6	Initial number of drops		
2.5 (m/s)	Maximum flow velocity		
0.001	Maximum longitudinal slope		
1:1 – 2:1	Side slope		
1	Soil shrinkage factor (ʎ)		
Volume-dependent cost			
Embankment		74100 (IRR/m^3)	
Cutting		193000 (IRR/m^3)	
Canal works		582000 (IRR/m^3)	
	Transportation cost for moving 1 m^3 of soil to landfill	9810 ($IRR/m^3/km$)	
Haul	Transportation cost for moving 1 m^3 of soil from borrow pit + loading	9810 ($IRR/m^3/km$) + 192000 (IRR/m^3)	
Length-dependent cost			
Lining	Bed width between (0.6–1.2 m)	4689000 (IRR/m^3)	
	Bed width > 1.2 m	4461000 (IRR/m^3)	
Trimming		76000 (IRR/m^2)	
Embedding longitudinal seams		111500 (IRR/dm^3)	
Preparation of materials and filling of concrete joints		38400 (IRR/dm^3)	
Construction-dependent cost			
Concreting hydraulic structures		3997000 (IRR/m^3)	
Reinforcement		137500 (IRR/kg)	
Framework		1540000 (IRR/m^2)	
Others			
Surcharge	Polishing	76400 (IRR/m^2)	
	Concreting in reinforced concrete	99800 (IRR/m^3)	
	Concreting hydraulic structures	507500 (IRR/m^3)	

of the optimization process. Figure 9 shows that the model has successfully passed the canal through the highland areas, significantly reducing the volume of earthworks. The optimal solution consists of three drops instead of six at the early stages of the process, which shows the ability of the proposed model to select the optimal number of drops. The values related to the distance and height difference of the drops are listed in Table 2. Along the optimal route, three drops with height differences of 7.30, 6.30, and 6.95 m and distances of 148.2 and 182.4 m from each other are considered the optimal option. Choosing the slope of the inclined part floating between the 2H:1V and 1.5H:1V range helps in reducing the penalty specified in Equation (11). Conversely, because the inclined slopes are within the permitted design range, it is operationally feasible. However, it needs more structural consideration, which is outside the scope of this paper. The position of the drops is chosen in steep areas, which facilitates the ease of implementation and

Figure 8
Route alignment and placement of RIDs in the (a) initial and (b) middle steps of the optimization process

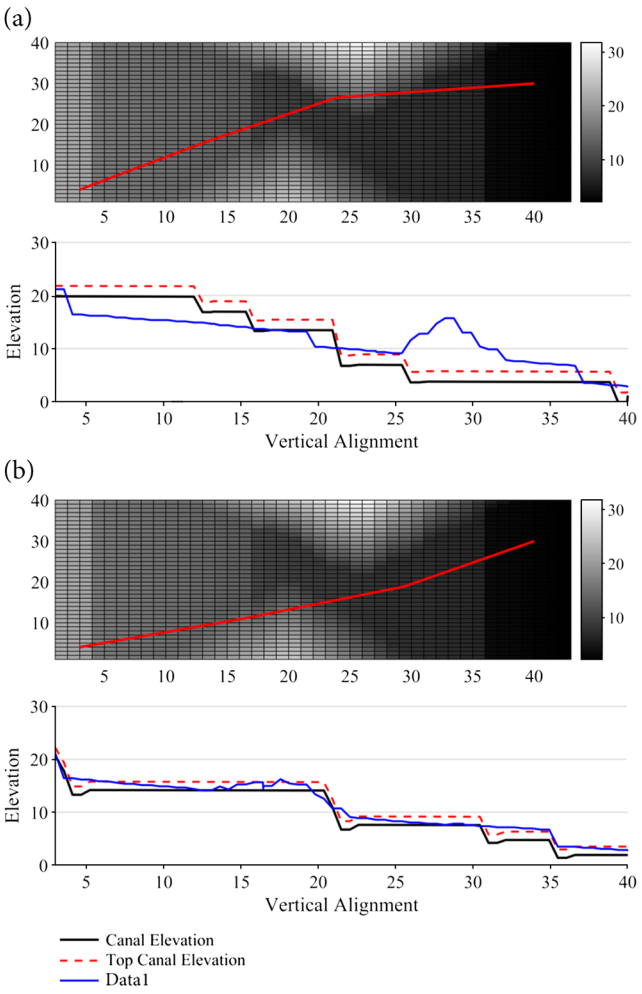

Figure 9
Optimized horizontal and vertical alignments at the 300th iteration of example 1

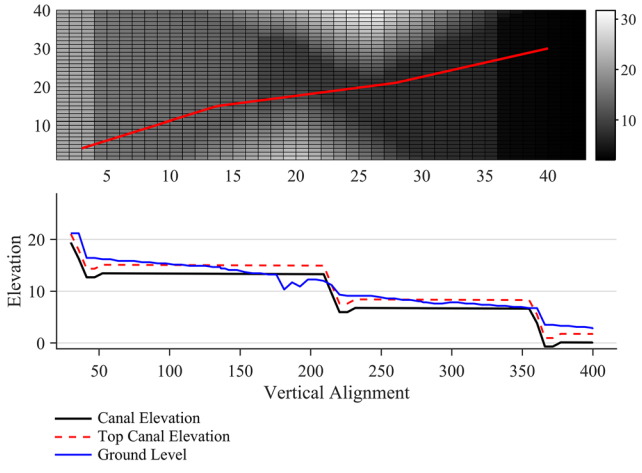

reduction of the construction costs. In Table 3, the cost items considered for drop construction are listed. The excavation-to-embankment ratio is a critical factor in construction planning and can significantly reduce earthwork costs. Assuming that the local soil is suitable for use and

Table 2
Outputs of the proposed model for example 1

Item	Value	Item	Value
Bottom width	1.2	Height of drops	7.26
Flow depth	0.95		6.30
Longitudinal slope	0.001		6.95
Side slope	1:1	Volume-dependent cost	1923.6
Velocity	1.48	Length-dependent cost	1610
Froude number	0.57	Construction-dependent cost	2499.4
Embankment	3877	Penalty cost	1.16
Cutting volume	3877	Total cost	6034.2
Distance between drops	148.2		
	182.4		

Note: *** It should be noted that the dimensions are in the SI unit and the costs are in rials.

Table 3
Example of cost-estimation output table for the ith RID

Items	Unit	Cost per unit	Amounts	Total cost
Canal work in different cross-sectional shapes with bottom widths less than 4 m	m^3	582000	27.996	16294205.12
Trimming and regulating the bed for lining	m^2	76000	0.4916	37367.8372
Excavation and transportation up to a distance of 50 m	m^3	193000	10.210	1970579.695
Spreading, spraying water, leveling, adjusting, and compacting embankment layers	m^3	74100	51.793	3837880.014
Preparation and implementation of concrete with washed sand and 250 kg of cement per cubic meter of concrete	m^3	3997000	10.595	42350168.17
Surcharge for concreting item if the concrete is used in reinforced concrete	m^3	99800	10.595	1057429.768
Surcharge for concreting item if the volume of each hydraulic structure is 4 to 10 m3	m^3	507500	10.595	5377210.494
Surcharge for concreting item to polish concrete surfaces of hydraulic structures exposed to water flow	m^2	76400	31.705	2422304.251
Reinforcement and rebar bending with a diameter of 12–18 mm for use in reinforced concrete	kg	137500	1792.2446	246433636
Framework	m^2	1540000	47.664	73403298.37

applying a compaction factor of 1, this ratio is taken as 1. Under this condition, transportation costs are limited to movement between sections, excluding loading expenses. For flow parameters, the canal is designed with a bed width of 1.2 m, a depth of 0.95 m, a longitudinal slope of 0.001, and a side slope of 1. The flow velocity is approximately 1.5 m/s, which falls within the standard range (0.6–2.5 m/s) for lined channels to prevent sedimentation and erosion. These dimensions also ensure that the Froude number remains within acceptable limits. On the basis of these assumptions and an iteration cap of 300, the model's average runtime was recorded at 304 s across 10 executions.

7.2. Example 2

In example 2, a continuous surface with varying slopes was constructed to evaluate the model's ability to optimize the placement and height of RIDs across different gradients. To achieve this, an artificial terrain was created with successive slopes of 0.16%, 1%, 2%, and 0.125% (Figure 10). In this case, the design discharge is equal to 10 m3/s, and the height difference between the starting and ending points of the route is equal to 12 m. Nine RIDs have been selected as the initial number at the beginning of the optimization process (Figure 11). Observing the optimal variant of the model for example 2 shows that it is needless to build a drop at the beginning and end of the path due to the

Figure 10
Ground profile for example 2

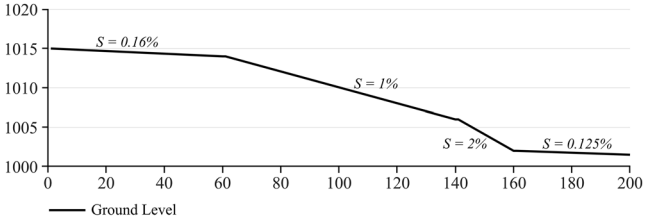

Figure 11
Total cost changes in successive iterations and the best vertical alignment for example 2

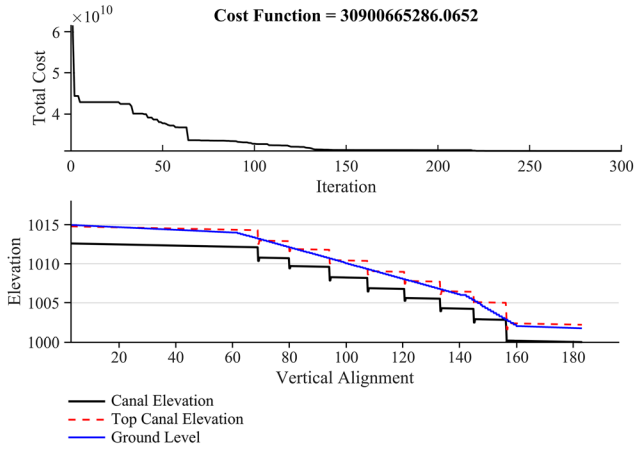

mild slope (Figure 10). The optimal option consists of seven drops with almost the same heights and distances in the area with a 1% slope and one drop with a height of 3 m in the area with a 2% slope, which can be a suitable option in this part due to its shortness (approximately 200 m) and steep terrain slope. The selection of a short and consecutive set of drops in relatively long routes with a uniform slope has reduced the volume of earthworks. In this section, the excavation-to-embankment ratio is 1.76, which, when compared to the overall ratio of 2.18, indicates a greater equilibrium in earthworks owing to the meticulous choice of RIDs. The aspect ratio (depth/bottom width) for this choice is 0.7. Although this ratio meets the technical and economic standards according to conventional principles, it can be deduced that the value obtained are unique for the least-cost feasible option, taking into account the available topography and other assumptions related to the problem. Table 4 and Table 5 show the model outputs of the optimal variant and cost estimation for the canal, excluding the structures, respectively. On the basis of the assumptions of this example, with 300 iterations and an approximate canal length of 200 m, the model's average runtime was recorded at 433 s over 10 executions. A comparison between examples 1 and 2 reveals that achieving an optimal design is not solely a matter of minimizing the number of drop structures along the route. Instead, it must account for topographic conditions, construction costs, and design constraints to ensure overall efficiency and feasibility.

7.3. Comparative performance analysis of PSO, GA, and ACO in the proposed optimization model

To assess the performance of the proposed PSO-based canal alignment optimization model, two other population-based metaheuristic algorithms— GA and ant colony optimization (ACO)—were evaluated under the same experimental conditions. Example 2 was selected as the test case due to its complex topography and variable slope profile, providing a challenging benchmark for comparative algorithm testing.

The evaluation centered on key performance metrics: the final objective function value, average computation time, and solution robustness across multiple independent runs.

As shown in Table 6, PSO consistently delivered the most favorable outcomes, yielding the lowest objective function values and exhibiting strong convergence behavior. Although GA achieved the shortest average runtime (398 s), the quality of its solutions was slightly inferior to those obtained with PSO. ACO, although capable of producing acceptable solutions, displayed higher variability and required extensive parameter tuning to achieve reliable performance.

In contrast, PSO demonstrated low sensitivity to initialization parameters and scaling, enhancing its reliability and ease of use. These results highlight PSO's practical advantages in solving complex, large-scale, nonlinear optimization problems—particularly in the domain of 3D canal alignment and optimal placement of RIDs.

7.4. A real-world example

To demonstrate the practical applicability of the proposed model, a real-world scenario was analyzed using actual project data. In this

Table 4
Outputs of the proposed model for example 2

Item	Value	Item	Value
Bottom width	2.18	Height of drops	**1.60**
Flow depth	1.53		**1.17**
Longitudinal slope	0.0007		**1.60**
Side slope	1:1		**1.60**
Velocity	1.76		**1.17**
Froude number	0.54		**1.60**
Embankment	10708		**1.60**
Cutting volume	23420		**3.20**
Distance between drops	104	**Dominant costs**	
	138	Volume-dependent cost	**13698**
	136	Length-dependent cost	**9823.5**
	114	Construction-dependent cost	**7740.7**
	132	Penalty cost	**44.6**
	120	Total cost	**31307**
	108		

Note: *** It should be noted that the dimensions are in SI units, and the costs are in million rials.

Table 5
Canal cost estimation table of the output of the optimization model

Cost items	Unit	Cost per unit	Amounts	Total cost
Demolition operation	m^2	790	35817.5871	28295893.81
Trimming and regulating the bed for lining	m^2	76000	1299.36612	98751824.79
Loading of materials from earthwork and its depletion	m^3	70000	12712.1488	889850416.8
Spreading, spraying water, leveling, adjusting, and compacting embankment layers	m^3	74100	10648.3902	789045714.8
Excavation of soil in any land for embankment	m^3	192000	0	0
Canal works	m^3	582000	19562.8512	11385579413
Excavation and transportation up to a distance of 50 m	m^3	193000	586.348778	113165314.2
Preparation of materials and implementation of concrete 250 kg of cement per cubic meter for lining	m^3	4461000	1459.71109	6511771168
Embedding of all types of seams in concrete works with all necessary materials and tools	dm^3	111500	36782.8655	4101289504
Transportation of materials obtained from excavation and canal digging for use in normal embankments	m^3_km	9180	12712.1488	116697526.1
Transportation cost for moving 1 m3 of soil from borrow pit	m^3_km	9180	0	0
Preparing materials and filling concrete joints with sand	dm^3	38400	38865.9231	1492451446

Table 6
Performance metrics of PSO, GA, and ACO algorithms

Criteria	PSO	GA	ACO
Objective value	2.7E+10	3.3E+10	3.6E+10
Best result	2.5E+10	2.9E+10	3.4E+10
Average runtime (s)	433	398	570
Population size	72	72	72
Iteration	300	300	300
Parameter sensitivity	Low	Medium	High

Table 7
Outputs of the proposed model in a real-world example

Outputs	Traditional method	Proposed model
Height (m)	2.68	2.95
	2.33	3.11
	1	-
Earthwork cut & fill (m^3)	2908.9	4281.9
	12219	6582
Total cost (million rials)	9600	8700

case, the optimization focused specifically on two critical parameters: the placement and height of the drops. By optimizing these variables, the total earthwork volume was reduced by 29%, primarily through the strategic adjustment of both the number and location of the drops. This reduction translated into a 9% decrease in the overall project execution cost.

These results highlight the model's effectiveness in achieving substantial cost and resource savings, even when applied to a single aspect of project design. A comparison with conventional methods, presented in Table 7, shows that the optimized model maintains an acceptable cut-to-fill ratio. Figure 12 further illustrates the difference in drop placement between the conventional approach and the optimized design.

8. Sensitivity Analysis

Choosing the appropriate values for the parameters of velocity, inertia weight, population, and individual and social learning coefficients of the PSO algorithm has a significant impact on the performance and efficiency of the algorithm. There is no specific method for the optimal selection of these values. It is determined based on the user's experience and the type of optimization problem [52]. In general, these coefficients should be chosen to maintain the trade-off between exploration and exploitation, which means helping the algorithm get rid of the local optimum and find the global optimum.

Figure 12
Placement of drops in the conventional and proposed models

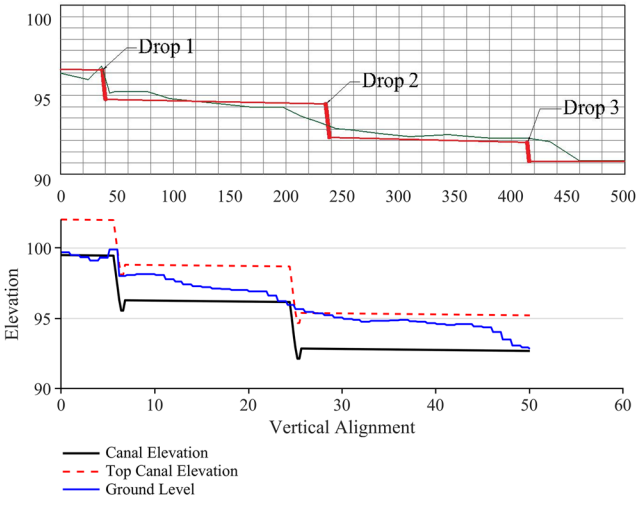

8.1. Swarm size

The swarm size or number of particles is influenced by both the number of decision variables and the complexity of the objective

function. Although a larger population can increase computational time, an overly small population may cause the algorithm to converge prematurely to a local optimum. Previous studies have shown that using fewer than 50 particles can significantly degrade the algorithm's performance [53]. Accordingly, this study ensures a minimum swarm size of 50, with adjustments made based on the number of variables involved to maintain adequate exploration capability.

8.2. Velocity modification and inertia weight

To ensure that particles remain within the defined search space, their velocity is constrained within a specific range. Excessively high velocities can destabilize the algorithm, whereas very low velocities increase the risk of premature convergence to a local optimum. To facilitate a smooth transition from the exploitation phase to the exploration phase, an inertia weight coefficient is employed to gradually reduce velocity over the course of the algorithm's execution.

In this study, experimental results suggest that an initial inertia weight of 0.9 and a damping coefficient of 0.99 significantly improve the algorithm's performance. Table 8 displays the objective function values from 10 independent runs under different velocity settings. The findings indicate that a velocity of 0.2 leads to premature convergence to a local optimum, reducing efficiency. Conversely, a velocity of 0.3 promotes more reliable convergence to the global optimum, enhancing overall algorithm performance.

8.3. Accelerator constant

In the PSO algorithm, cognitive (C_1) and social components (C_2) are accelerators that enable particles to share their best individual and global experiences in the search space. Choosing large values of cognitive coefficients compared with the social component leads to the wandering of the particles in the search space [54]. In addition, choosing higher values of the social component (C_2) than the cognitive component (C_1) leads to the rapid movement of particles to the local optimum [55]. Different values of C_1 and C_2 were calculated using the relationship $C_1 = 4\text{-}C_2$, for $C_2 = [1.5\ 1.7\ 2\ 2.3\ 2.5]$, and applied in the model. Figure 13 shows the maximum, minimum, and average values of the objective function for 10 times of running the model for each pair of accelerator coefficients. The results show that the objective function moves away from the global optimum when the values of C_1 and C_2 are chosen significantly more than 2 (C_2>2>C_1) or (C_1>2>C_2). In contrast, the reduction of this difference leads to an improvement in the algorithm's performance. Therefore, as mentioned above, applying constant 2 for both C_1 and C_2 enhances the model's performance and provides a better solution.

8.4. Summary of the model performance

The proposed 3D optimization model—integrating PSO with GIS capabilities—was benchmarked against traditional canal design methods to assess its performance. Unlike conventional approaches that often depend on manual alignments and heuristic adjustments, this model automates the generation of multiple alignment alternatives and systematically identifies the most cost-effective route and cross-sectional parameters all while adhering to hydraulic and design constraints.

The model demonstrated a clear advantage in optimizing the placement and height of RIDs. In synthetic test scenarios, it effectively filtered out suboptimal solutions and adapted to varying terrain characteristics. For example, in the first test case, reducing the number of drops led to significant cost savings, and the second scenario showed that using more frequent, lower-height drops produced better results—demonstrating the model's ability to tailor solutions dynamically to site-specific conditions.

When applied to a real-world case, the model achieved a 9% reduction in implementation costs compared to conventional methods, solely through optimized drop placement—even with limited input data. This highlights its superior performance in practical settings. The combination of cost efficiency, adaptability, and automated analysis positions the model as a valuable decision-support tool for preliminary canal alignment planning. Its use of a continuous search space and GIS-driven variant generation sets it apart from previous methodologies, enabling more precise and economically optimized designs, particularly for sloped and complex terrains.

Table 8
Variation of cost functions against velocities

Velocity	0.2	0.3	0.4	0.5
Number of runs		**Cost function (IRR)**		
1	6.29E+09	5.90E+09	6.38E+09	6.38E+09
2	6.32E+09	7.41E+09	7.10E+09	8.09E+09
3	7.34E+09	6.58E+09	6.16E+09	7.29E+09
4	6.34E+09	6.21E+09	6.24E+09	6.66E+09
5	6.67E+09	6.08E+09	6.52E+09	7.39E+09
6	6.62E+09	7.03E+09	7.71E+09	7.25E+09
7	6.96E+09	6.54E+09	7.17E+09	6.60E+09
8	7.05E+09	5.96E+09	6.78E+09	7.24E+09
9	6.21E+09	6.03E+09	6.77E+09	6.72E+09
10	6.64E+09	6.67E+09	6.16E+09	6.87E+09
Average	6.59E+09	**6.44E+09**	6.48E+09	7.16E+09
Max	7.34E+09	7.41E+09	**7.10E+09**	8.09E+09
Min	6.21E+09	5.90E+09	6.16E+09	6.38E+09

Figure 13
Variation of the cost function against the values of the accelerator components (C_1 & C_2)

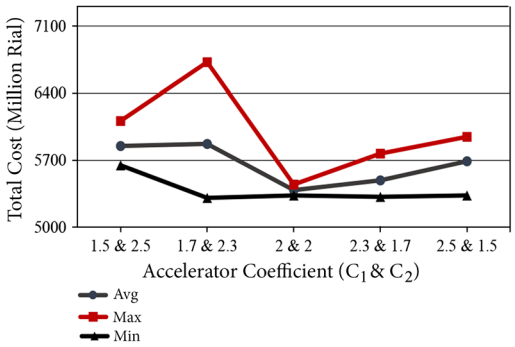

9. Conclusion

This research presents a novel 3D optimization model that integrates a PSO algorithm with a GIS to address the challenge of designing canal alignments on sloping terrains. The primary objective is to minimize associated costs while satisfying engineering and hydraulic design constraints. The model automatically generates multiple alignment alternatives and identifies the most economically viable canal route along with optimal flow section parameters. It also determines the best placement and height of RIDs, balancing both construction feasibility and hydraulic requirements.

The model's performance was evaluated through two synthetic case studies using artificial terrain layers and one real-world application. Results confirmed the model's ability to overcome terrain-related constraints, discard suboptimal configurations, and identify cost-effective solutions. In the first example, reducing the number of drops led to a noticeable decrease in implementation costs. In contrast, the second example showed that a higher number of lower-height RIDs yielded the most efficient design. These outcomes underscore the model's adaptability and intelligence in dynamically optimizing drop placement based on specific terrain conditions.

In the real-world scenario, despite limited input data, the model achieved a 9% reduction in implementation costs compared to conventional design approaches—purely through optimization of drop location and height. This highlights the model's capability to meet both economic and technical objectives.

The continuous search space, coupled with GIS-based variant generation, enhances the model's ability to automate early-stage design and deliver optimized canal alignments in complex terrains. Future research may further refine the model by incorporating additional real-world datasets and broader design parameters.

Conflicts of Interest

Manoj K. Jha is an Associate Editor for *Journal of Computational and Cognitive Engineering*, and was not involved in the editorial review or the decision to publish this article. The authors declare that they have no conflicts of interest to this work.

Data Availability Statement

Data sharing is not applicable to this article as no new data were created or analyzed in this study.

Author Contribution Statement

Mehdi Kazemi: Conceptualization, Methodology, Software, Formal analysis, Investigation, Resources, Data curation, Writing – original draft, Visualization. **Ebrahim Amiri Tokaldani:** Conceptualization, Methodology, Validation, Formal analysis, Resources, Data curation, Writing – original draft, Supervision, Project administration. **Manoj K. Jha:** Conceptualization, Methodology, Validation, Formal analysis, Writing – original draft, Writing – review & editing, Supervision, Project administration. **Ramesh Rudra:** Validation, Supervision, Project administration.

References

[1] Wan, X., Pu, H., Schonfeld, P., Song, T., Li, W., & Peng, L. (2024). Railway alignment optimization in regions with densely-distributed obstacles based on semantic topological maps. *Integrated Computer-Aided Engineering*, *31*(4), 421–437. https://doi.org/10.3233/ICA-240739

[2] Song, T., Pu, H., Schonfeld, P., & Hu, J. (2023). Railway alignment optimization under uncertainty with a minimax robust method. *IEEE Intelligent Transportation Systems Magazine*, *15*(1), 333–346. https://doi.org/10.1109/MITS.2022.3146143

[3] Al-Hadad, B. M. A., Nadir, W. H., & Jukil, G. A. M. (2024). Intelligent optimization of highway alignments: A novel approach integrating geographic information system and genetic algorithms. *Engineering Applications of Artificial Intelligence*, *133*, 108037. https://doi.org/10.1016/j.engappai.2024.108037

[4] Shafahi, Y., & Bagherian, M. (2013). A customized particle swarm method to solve highway alignment optimization problem. *Computer-Aided Civil and Infrastructure Engineering*, *28*(1), 52–67. https://doi.org/10.1111/j.1467-8667.2012.00769.x

[5] Dissanayaka, G. D. V. C., & Pushpakumara, T. D. C. (2025). Road alignment optimization in landslide-prone areas: A GIS-based approach in Yatiyanthota, Sri Lanka. *International Journal of Innovative Science and Research Technology*, *10*(3), 1713–1719. https://doi.org/10.38124/ijisrt/25mar1138

[6] Kang, M.-W., Jha, M. K., & Schonfeld, P. (2012). Applicability of highway alignment optimization models. *Transportation Research Part C: Emerging Technologies*, *21*(1), 257–286. https://doi.org/10.1016/j.trc.2011.09.006

[7] Ferdowsi, A., Valikhan-Anaraki, M., Mousavi, S.-F., Farzin, S., & Mirjalili, S. (2021). Developing a model for multi-objective optimization of open channels and labyrinth weirs: Theory and application in Isfahan irrigation networks. *Flow Measurement and Instrumentation*, *80*, 101971. https://doi.org/10.1016/j.flowmeasinst.2021.101971

[8] Niazkar, M. (2020). Assessment of artificial intelligence models for calculating optimum properties of lined channels. *Journal of Hydroinformatics*, *22*(5), 1410–1423. https://doi.org/10.2166/hydro.2020.050

[9] Niazkar, M. (2021). Optimum design of straight circular channels incorporating constant and variable roughness scenarios: Assessment of machine learning models. *Mathematical Problems in Engineering*, *2021*(1), 9984934. https://doi.org/10.1155/2021/9984934

[10] Salem, A. K., Imam, Y. E., Ghanem, A. H., & Bazaraa, A. S. (2022). Genetic algorithm based model for optimal selection of open channel design parameters. *Water Resources Management*, *36*(15), 5867–5896. https://doi.org/10.1007/s11269-022-03323-w

[11] Rahman, S. H., & Sarma, B. (2023). Optimization of Sukla Irrigation Canal. In *Sustainable Water Resources Management: Proceedings of SWARM 2020*, 118–130. https://doi.org/10.1007/978-981-16-7535-5_13

[12] Roushangar, K., Alami, M. T., Nourani, V., & Nouri, A. (2017). A cost model with several hydraulic constraints for optimizing in

practice a trapezoidal cross section. *Journal of Hydroinformatics*, *19*(3), 456–468. https://doi.org/10.2166/hydro.2017.081

[13] Swamee, P. K., Mishra, G. C., & Chahar, B. R. (2000). Minimum cost design of lined canal sections. *Water Resources Management*, *14*(1), 1–12. https://doi.org/10.1023/A:1008198602337

[14] Jain, A., Bhattacharjya, R. K., & Sanaga, S. (2004). Optimal design of composite channels using genetic algorithm. *Journal of Irrigation and Drainage Engineering*, *130*(4), 286–295. https://doi.org/10.1061/(ASCE)0733-9437(2004)130:4(286)

[15] Depeweg, H., & Urquieta, E. R. (2004). GIS tools and the design of irrigation canals. *Irrigation and Drainage*, *53*(3), 301–314. https://doi.org/10.1002/ird.112

[16] Aksoy, B., & Altan-Sakarya, A. B. (2006). Optimal lined channel design. *Canadian Journal of Civil Engineering*, *33*(5), 535–545. https://doi.org/10.1139/l06-008

[17] Turan, M. E., & Yurdusev, M. A. (2011). Optimization of open canal cross sections by differential evolution algorithm. *Mathematical and Computational Applications*, *16*(1), 77–86.

[18] Tofiq, F. A., & Guven, A. (2015). Optimal design of trapezoidal lined channel with least cost: Semi-theoretical approach powered by genetic programming. *Water SA*, *41*(4), 483–489. http://dx.doi.org/10.4314/wsa.v41i4.07

[19] El-Ghandour, H. A., Elbeltagi, E., & Gabr, M. E. (2020). Design of irrigation canals with minimum overall cost using particle swarm optimization—Case study: El-sheikh Gaber canal, north Sinai Peninsula, Egypt. *Journal of Hydroinformatics*, *22*(5), 1258–1269. https://doi.org/10.2166/hydro.2020.199

[20] Ponnathota, S. C. R., & Rajan, K. S. (2023). Topology aligned least cost routing model for canals. In *2023 IEEE International Geoscience and Remote Sensing Symposium*, 3024–3027. https://doi.org/10.1109/IGARSS52108.2023.10282779

[21] Castro, A., Casal, G., Santamarina, D., & Vázquez-Méndez, M. E. (2025). A simple method for automatic recreation of railway horizontal alignments. *Railway Engineering Science*, *33*(1), 62–78. https://doi.org/10.1007/s40534-024-00348-2

[22] Vázquez-Méndez, M. E., Casal, G., Castro, A., & Santamarina, D. (2021). An algorithm for random generation of admissible horizontal alignments for optimum layout design. *Computer-Aided Civil and Infrastructure Engineering*, *36*(8), 1056–1072. https://doi.org/10.1111/mice.12682

[23] Aftabi Hossein, S., & Rahimov, K. (2023). Balancing environmental and economic considerations in horizontal alignment optimization of a ring road near Anzali International Wetland. *Environmental Energy and Economic Research*, *7*(3), 1–23. https://doi.org/10.22097/eeer.2023.396033.1290

[24] Kurhan, M., Kurhan, D., & Hmelevska, N. (2024). Innovative approaches to railway track alignment optimization, in curved sections. *Acta Polytechnica Hungarica*, *21*(1), 207–220.

[25] Jiang, L., Li, W., Jiang, L., Wang, Z., & Wen, T. (2025). Railway alignment optimization and seismic responses of high-speed railway bridge considering the spatial effects of mountainous-plateau. *International Journal of Structural Stability and Dynamics*, *25*(16), 2550170. https://doi.org/10.1142/S0219455425501706

[26] Wu, X., Fu, S., & Guo, L. (2023). Study on highway alignment optimization considering rollover stability based on two-dimensional point collision dynamics. *Applied Sciences*, *13*(1), 509. https://doi.org/10.3390/app13010509

[27] Momo, N. S., Hare, W., & Lucet, Y. (2023). Modeling side slopes in vertical alignment resource road construction using convex optimization. *Computer-Aided Civil and Infrastructure Engineering*, *38*(2), 211–224. https://doi.org/10.1111/mice.12879

[28] Sushma, M. B., Roy, S., & Maji, A. (2022). Exploring and exploiting ant colony optimization algorithm for vertical highway alignment development. *Computer-Aided Civil and Infrastructure Engineering*, *37*(12), 1582–1601. https://doi.org/10.1111/mice.12814

[29] Kim, M. E., & Kim, E. (2020). Simulation-based multistage optimization model for railroad alignment design and operations. *Journal of Transportation Engineering, Part A: Systems*, *146*(7), 04020057. https://doi.org/10.1061/JTEPBS.0000380

[30] Yang, D., Wang, H., Yi, S., & He, Q. (2025). *Alignment optimization in rail transit*. Switzerland: Springer Nature. https://doi.org/10.1007/978-3-031-80561-5

[31] Jha, M. K., & Schonfeld, P. (2000). Integrating genetic algorithms and geographic information system to optimize highway alignments. *Transportation Research Record: Journal of the Transportation Research Board*, *1719*(1), 233–240. https://doi.org/10.3141/1719-31

[32] Ghanizadeh, A. R., Heidarabadizadeh, N., & Mahmoodabadi, M. J. (2020). Effect of objective function on the optimization of highway vertical alignment by means of metaheuristic algorithms. *Civil Engineering Infrastructures Journal*, *53*(1), 115–136. https://doi.org/10.22059/ceij.2019.279837.1578

[33] You, K., Yu, Q., Huang, W., & Hu, Y. (2022). Safety-based optimization model for highway horizontal alignment design. *Mathematical Problems in Engineering*, *2022*(1), 6214910. https://doi.org/10.1155/2022/6214910

[34] Gao, Y., Zhang, T., Wang, Q., Yang, S., Zhuo, J., Tang, J., …, & He, Q. (2023). Low-construction-emissions optimization for railway alignment fine-grained designs within densely populated urban areas. *Construction and Building Materials*, *366*, 130179. https://doi.org/10.1016/j.conbuildmat.2022.130179

[35] Biancardo, S. A., Avella, F., di Lisa, E., Chen, X., Abbondati, F., & Dell'Acqua, G. (2021). Multiobjective railway alignment optimization using ballastless track and reduced cross-section in tunnel. *Sustainability*, *13*(19), 10672. https://doi.org/10.3390/su131910672

[36] Isler, C. A., & Widmer, J. A. (2020). Parallel genetic algorithm and high performance computing to solve the intercity railway alignment optimization problem. In M. Marinov & J. Piip (Eds.), *Sustainable rail transport* (pp. 159–186). Springer International Publishing. https://doi.org/10.1007/978-3-030-19519-9_5

[37] Henderson, F. M. (1966). *Open channel flow*. USA: Macmillan.

[38] Aisenbrey, A. (1974). *Design of small canal structures: Engineering technology pertaining primarily to the design of small canal structures of less than 100-cubic-feet-per-second capacity*. USA: United States Department of the Interior.

[39] Novák, P., Moffat, A., Nalluri, C., & Narayanan, R. (2017). *Hydraulic structures* (4th ed.). USA: CRC Press. https://doi.org/10.1201/9781315274898

[40] United States Department of the Interior Bureau of Reclamation. (1964). *Design standards No. 3: Canals and related structures*. United States Department of the Interior, Bureau of Reclamation. https://www.usbr.gov/pn/snakeriver/landuse/authorized/designstandards3.pdf

[41] Shami, T. M., Mirjalili, S., Al-Eryani, Y., Daoudi, K., Izadi, S., & Abualigah, L. (2023). Velocity pausing particle swarm optimization: A novel variant for global optimization. *Neural*

Computing and Applications, *35*(12), 9193–9223. https://doi.org/10.1007/s00521-022-08179-0

[42] Zhao, F., Ji, F., Xu, T., Zhu, N., & Jonrinaldi. (2024). Hierarchical parallel search with automatic parameter configuration for particle swarm optimization. *Applied Soft Computing*, *151*, 111126. https://doi.org/10.1016/j.asoc.2023.111126

[43] Farzin, S., & Valikhan Anaraki, M. (2021). Optimal construction of an open channel by considering different conditions and uncertainty: Application of evolutionary methods. *Engineering Optimization*, *53*(7), 1173–1191. https://doi.org/10.1080/0305215X.2020.1775825

[44] Wang, H., Xie, P., Li, Z., & Gao, J. (2024). Highway alignment optimization design method based on multi-objective particle swarm optimization. *E3S Web of Conferences*, *512*, 03005. https://doi.org/10.1051/e3sconf/202451203005

[45] van Zyl, J. P., & Engelbrecht, A. P. (2023). Set-based particle swarm optimisation: A review. *Mathematics*, *11*(13), 2980. https://doi.org/10.3390/math11132980

[46] Gad, A. G. (2022). Particle swarm optimization algorithm and its applications: A systematic review. *Archives of Computational Methods in Engineering*, *29*(5), 2531–2561. https://doi.org/10.1007/s11831-021-09694-4

[47] Clerc, M. (1999). The swarm and the queen: Towards a deterministic and adaptive particle swarm optimization. In *Proceedings of the 1999 Congress on Evolutionary Computation-CEC99*, 1951–1957. https://doi.org/10.1109/CEC.1999.785513

[48] Ezugwu, A. E., Agushaka, J. O., Abualigah, L., Mirjalili, S., & Gandomi, A. H. (2022). Prairie dog optimization algorithm. *Neural Computing and Applications*, *34*(22), 20017–20065. https://doi.org/10.1007/s00521-022-07530-9

[49] Song, Y., Liu, Y., Chen, H., & Deng, W. (2023). A multi-strategy adaptive particle swarm optimization algorithm for solving optimization problem. *Electronics*, *12*(3), 491. https://doi.org/10.3390/electronics12030491

[50] Shami, T. M., El-Saleh, A. A., Alswaitti, M., Al-Tashi, Q., Summakieh, M. A., & Mirjalili, S. (2022). Particle swarm optimization: A comprehensive survey. *IEEE Access*, *10*, 10031–10061. https://doi.org/10.1109/ACCESS.2022.3142859

[51] Zhang, Y., & Kong, X. (2023). A particle swarm optimization algorithm with empirical balance strategy. *Chaos, Solitons & Fractals: X*, *10*, 100089. https://doi.org/10.1016/j.csfx.2022.100089

[52] Shi, Y. (2004). Particle swarm optimization. *IEEE Connections*, *2*(1), 8–13.

[53] Dong, Y., Tang, J., Xu, B., & Wang, D. (2005). An application of swarm optimization to nonlinear programming. *Computers & Mathematics with Applications*, *49*(11–12), 1655–1668. https://doi.org/10.1016/j.camwa.2005.02.006

[54] Kennedy, J., & Eberhart, R. (1995). Particle swarm optimization. In *Proceedings of ICNN'95-International Conference on Neural Networks*, 1942–1948. https://doi.org/10.1109/ICNN.1995.488968

[55] Perez, R. E., & Behdinan, K. (2007). Particle swarm approach for structural design optimization. *Computers & Structures*, *85*(19–20), 1579–1588. https://doi.org/10.1016/j.compstruc.2006.10.013

How to Cite: Kazemi, M., Tokaldani, E. A., Jha, M. K., & Rudra, R. (2026). A 3D Irrigation Canal Alignment Optimization Model for a Steep-Sloping Area with Rectangular Inclined Drops. *Journal of Computational and Cognitive Engineering*, *5*(1), 30–43. https://doi.org/10.47852/bonviewJCCE52024527